Article

X-ray polarization evidence for a 200-year-old flare of Sgr A*

https://doi.org/10.1038/s41586-023-06064-x

Received: 25 November 2022

Accepted: 7 April 2023

Published online: 21 June 2023

Check for updates

Frédéric Marin[1]✉, Eugene Churazov[2,3], Ildar Khabibullin[2,3,4], Riccardo Ferrazzoli[5], Laura Di Gesu[6], Thibault Barnouin[1], Alessandro Di Marco[5], Riccardo Middei[7,8], Alexey Vikhlinin[3,9], Enrico Costa[5], Paolo Soffitta[5], Fabio Muleri[5], Rashid Sunyaev[2,3], William Forman[9], Ralph Kraft[9], Stefano Bianchi[10], Immacolata Donnarumma[6], Pierre-Olivier Petrucci[11], Teruaki Enoto[12], Iván Agudo[13], Lucio A. Antonelli[7,8], Matteo Bachetti[14], Luca Baldini[15,16], Wayne H. Baumgartner[17], Ronaldo Bellazzini[15], Stephen D. Bongiorno[17], Raffaella Bonino[18,19], Alessandro Brez[15], Niccolò Bucciantini[20,21,22], Fiamma Capitanio[5], Simone Castellano[15], Elisabetta Cavazzuti[6], Chien-Ting Chen[23], Stefano Ciprini[7,24], Alessandra De Rosa[5], Ettore Del Monte[5], Niccolò Di Lalla[25], Victor Doroshenko[26], Michal Dovčiak[27], Steven R. Ehlert[17], Yuri Evangelista[5], Sergio Fabiani[5], Javier A. Garcia[28], Shuichi Gunji[29], Kiyoshi Hayashida[30], Jeremy Heyl[31], Adam Ingram[32], Wataru Iwakiri[33,34], Svetlana G. Jorstad[35,36], Philip Kaaret[17,37], Vladimir Karas[27], Takao Kitaguchi[12], Jeffery J. Kolodziejczak[17], Henric Krawczynski[38], Fabio La Monaca[5], Luca Latronico[18], Ioannis Liodakis[39], Simone Maldera[18], Alberto Manfreda[15], Andrea Marinucci[6], Alan P. Marscher[35], Herman L. Marshall[40], Francesco Massaro[18,19], Giorgio Matt[10], Ikuyuki Mitsuishi[41], Tsunefumi Mizuno[42], Michela Negro[43,44,45], C.-Y. Ng[46], Stephen L. O'Dell[17], Nicola Omodei[25], Chiara Oppedisano[18], Alessandro Papitto[8], George G. Pavlov[47], Abel L. Peirson[25], Matteo Perri[7,8], Melissa Pesce-Rollins[15], Maura Pilia[14], Andrea Possenti[14], Juri Poutanen[48], Simonetta Puccetti[7], Brian D. Ramsey[17], John Rankin[5], Ajay Ratheesh[5], Oliver J. Roberts[23], Roger W. Romani[25], Carmelo Sgrò[15], Patrick Slane[9], Gloria Spandre[15], Doug Swartz[23], Toru Tamagawa[12], Fabrizio Tavecchio[49], Roberto Taverna[50], Yuzuru Tawara[41], Allyn F. Tennant[17], Nicholas E. Thomas[17], Francesco Tombesi[24,51,52], Alessio Trois[14], Sergey S. Tsygankov[48], Roberto Turolla[50,53], Jacco Vink[54], Martin C. Weisskopf[17], Kinwah Wu[53], Fei Xie[5,55] & Silvia Zane[53]

The centre of the Milky Way Galaxy hosts a black hole with a solar mass of about 4 million (Sagittarius A* (Sgr A)) that is very quiescent at present with a luminosity many orders of magnitude below those of active galactic nuclei[1]. Reflection of X-rays from Sgr A* by dense gas in the Galactic Centre region offers a means to study its past flaring activity on timescales of hundreds and thousands of years[2]. The shape of the X-ray continuum and the strong fluorescent iron line observed from giant molecular clouds in the vicinity of Sgr A* are consistent with the reflection scenario[3–5]. If this interpretation is correct, the reflected continuum emission should be polarized[6]. Here we report observations of polarized X-ray emission in the direction of the molecular clouds in the Galactic Centre using the Imaging X-ray Polarimetry Explorer. We measure a polarization degree of 31% ± 11%, and a polarization angle of −48° ± 11°. The polarization angle is consistent with Sgr A* being the primary source of the emission, and the polarization degree implies that some 200 years ago, the X-ray luminosity of Sgr A* was briefly comparable to that of a Seyfert galaxy.

The Imaging X-ray Polarimetry Explorer (IXPE) observed the molecular complex Sgr A, the X-ray-brightest group of reflection clouds near Sgr A* (ref. 7), for an exposure of 0.93 Ms after filtering in February and March 2022. Contemporaneous Chandra X-ray Observatory observations with high angular resolution were acquired to identify regions where the reflected emission is strong and to extract spectra from these regions. Figure 1 shows the X-ray surface brightness maps in the 4–8-keV band obtained. We excluded X-rays below 4 keV as they arise from unpolarized plasma emission[8–10] (Extended Data Fig. 2). See the Methods for details on the observations and data reduction.

On the basis of the Chandra image alone, we selected a circular extraction region with a radius of 4.5′ centred on the Sgr A complex that contains numerous hotspots of reflected emission (that is, scattering clouds). This region was selected to collect as many 'reflected' photons as possible while avoiding the edges of the IXPE detectors. The region includes most areas of elevated reflected emission. The region excludes

A list of affiliations appears at the end of the paper.

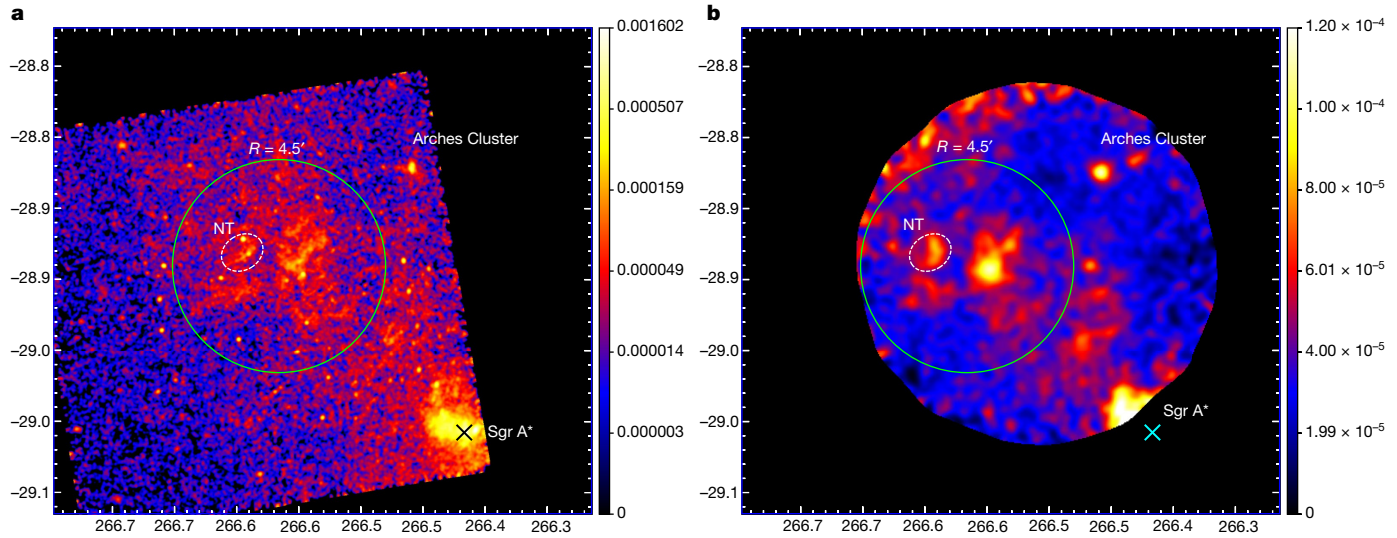

Fig. 1 | Quasi-simultaneous Chandra and IXPE 4–8-keV X-ray surface brightness maps of the Galactic Centre region to the northeast of Sgr A*. The Chandra (a) and IXPE (b) 4–8-keV X-ray surface brightness maps are in equatorial coordinates; north is up. The IXPE image is in units of counts per second per square arcminute per square centrimetre colour-coded on a linear scale (see the colour bar on the right). For IXPE, the edges of the image, where the exposure (including vignetting effects) drops below 15% of the maximal value, have been truncated[26]. For Chandra, the image units are the same as those for the IXPE image, but a logarithmic scale is used to show both diffuse and compact sources. The positions of the supermassive black hole Sgr A* and the Arches star cluster are labelled. The area where reflection emission is strong in the Chandra data is shown using a green circle with a radius of 4.5′. This circle was used to extract *I*, *Q* and *U* spectra from the IXPE data. The same region was used for Chandra and XMM-Newton spectral analysis. The white dashed ellipse shows the location of a bright non-thermal (NT) source G0.13-0.11 (ref. 11) that was excluded for the spectra extraction.

areas affected by very bright sources that enter the IXPE field of view as a result of the pointing dithering pattern and a bright1′ region associated with the non-thermal object G0.13-0.11 (ref. 11) to avoid possible contamination of the polarized signal.

Figure 2 shows good agreement between the spectra extracted from IXPE, Chandra and archival XMM-Newton data for the selected region. A bump, associated with iron lines at 6.4 and 6.7 keV, is clearly seen, even with IXPE's lower spectral resolution. The model based on XMM-Newton and Chandra data describes the IXPE spectrum well, given the current level of cross-calibration uncertainties between the instruments.

The spectral model is built from several components: thermal and reflected emission, fluorescent lines and scattered continuum (see Methods). All of them, except for the component representing the reflected emission from the molecular cloud, are assumed to be constant in time (that is, the same for all three datasets). The reflected emission is a combination of Compton-scattered and photo-absorbed continuum components with fluorescent emission lines calculated self-consistently from the reflection spectrum[12]. Only the continuum part of the reflected spectrum is expected to be polarized[9,10,13]. Hence, the X-ray polarization (described by the Stokes parameters *Q* and *U* measured by IXPE) is related to the reflection continuum $I_{\mathrm{refl,c}}$, and not to the total observed intensity *I* (refs. 14,15). The polarization degree is independent of photon energy in the single-scattering scenario, so the spectral shape of *Q* and *U* follow that of $I_{\mathrm{refl,c}}$.

Figure 3 shows the observed *Q* and *U* spectra. The *Q* values are close to zero, whereas *U* is mostly negative, suggesting a polarization angle close to −45°. The best-fitting reflection model is shown with solid lines. Here we have explicitly assumed that all emission from the selected region has the same polarization degree and angle, which is valid if the illuminated group of clouds is compact in three dimensions. With these simplifying assumptions, our model has only two free parameters derived from the IXPE data: degree of polarization $P = 31 \pm 11\%$ and polarization angle $\phi = -48° \pm 11°$ (uncertainties are 68% confidence level (Fig. 4); ϕ is anticlockwise from north in the equatorial coordinate system as per the convention of the International Astronomical Union). As explained in the Methods, the absolute normalization of the reflected component has about 30% uncertainty. Therefore, the constraints on the polarization degree are a multiplicative combination of statistical and systematic uncertainties: $P = (0.31 \pm 0.11)_{\mathrm{stat}} \times (1.0 \pm 0.3)_{\mathrm{sys}}$. Even with this extra uncertainty, it is clear that the observed polarization degree is substantially smaller than 100%. The systematic uncertainty does not affect the significance of the polarized signal detection, which corresponds to about 2.8 standard deviations.

The measured polarization angle ϕ is consistent with the hypothesis that Sgr A* is the primary source (Fig. 4). For a cloud located at the centre of our extraction region, the line orthogonal to the direction towards Sgr A* corresponds to $\phi = -42°$. This is within the uncertainties of our measurement ($\phi = -48° \pm 11°$), so fixing the measured polarization angle to −42° does not affect the errors on the degree of polarization.

The degree of polarization *P* of the reflected continuum is directly related to the scattering angle θ in the single-scattering approximation, $P = (1-\mu^2)/(1+\mu^2)$, in which $\mu = \cos\theta$. Any value of *P* produces two solutions, θ and $\pi - \theta$. For $P = 31 \pm 11\%$, the solutions are 43^{+7}_{-8} and 137^{+7}_{-8} degrees. A similar level of uncertainty is caused by the systematic error of about 30% in the value of *P*. These angles fix the scattering geometry; the smaller value corresponds to clouds between us and the primary source and the larger to clouds beyond the source (see Methods).

For a given scattering angle θ, one can also calculate the age of the flare t_{flare} (that is, the time delay associated with the propagation of X-rays from the primary source to the cloud and then to the observer). Adopting a projected distance between Sgr A* and the scattering clouds of 25 pc (that is, the distance between the supermassive black hole and the centre of our extraction zone in the sky plane), the two solutions for θ translate into two t_{flare} values: 33^{+6}_{-7} and 205^{+50}_{-30} years, respectively. Again, the systematic uncertainties are comparable to the quoted statistical errors (see Methods). From the point of view of polarization properties, both solutions are equivalent. However, the 'older' flare is far more plausible. First, for the cloud located well behind the primary source, the propagation speed of the light front of the flare approaches *c*/2 (ref. 16), in which *c* is the speed of light, whereas for the cloud in front of the primary source, this speed is always greater than *c*. Thus,

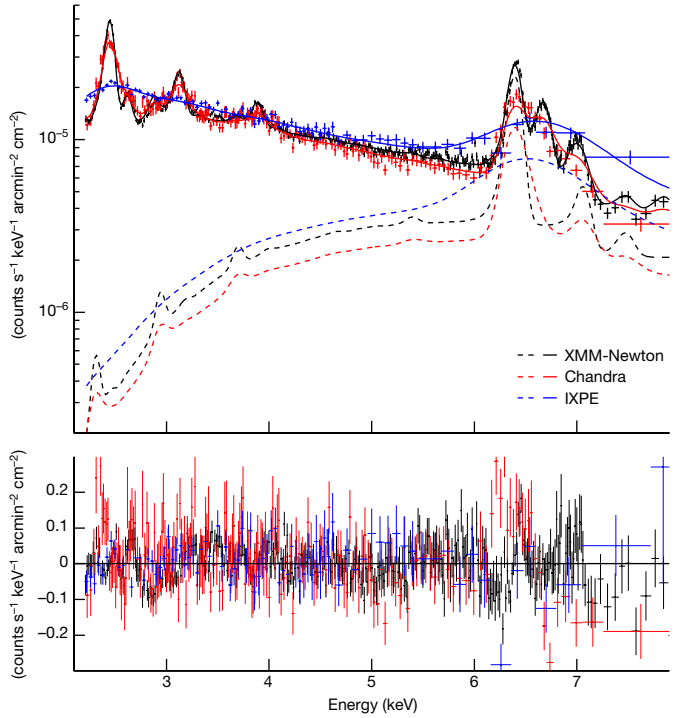

Fig. 2 | Spectra of the X-ray emission extracted from the circular region shown in Fig. 1 obtained in Chandra, IXPE and archival XMM-Newton observations, after division by the energy-dependent effective area of each telescope. The Chandra spectrum is in red, IXPE spectrum in blue and XMM-Newton spectrum in black (top panel). Error bars correspond to 1σ (68% confidence intervals). The solid lines correspond to the best-fitting models (three thermal components and the reflection emission, see Methods) convolved with the telescopes' spectral responses, resulting in strong smearing of the emission lines in the IXPE data. Parameters of the thermal components were fixed among all three datasets, and only the normalization of the reflection component was allowed to vary between them. The dashed lines show the best-fitting contribution of the reflected emission to the total spectrum for each of the three instruments. The difference in the normalization of the reflected emission (about 30%) could be caused by the time variability and the different energy-dependent efficiencies of the three telescopes. As demonstrated by the residuals shown in the second panel ((data-model)/model, bottom panel), the model provides a reasonable approximation of the data (at the level of about 20%) even although with high statistics of the XMM-Newton and Chandra data a few wiggles near the bright emission lines are visible, which are plausibly caused by slight gain variations among the datasets.

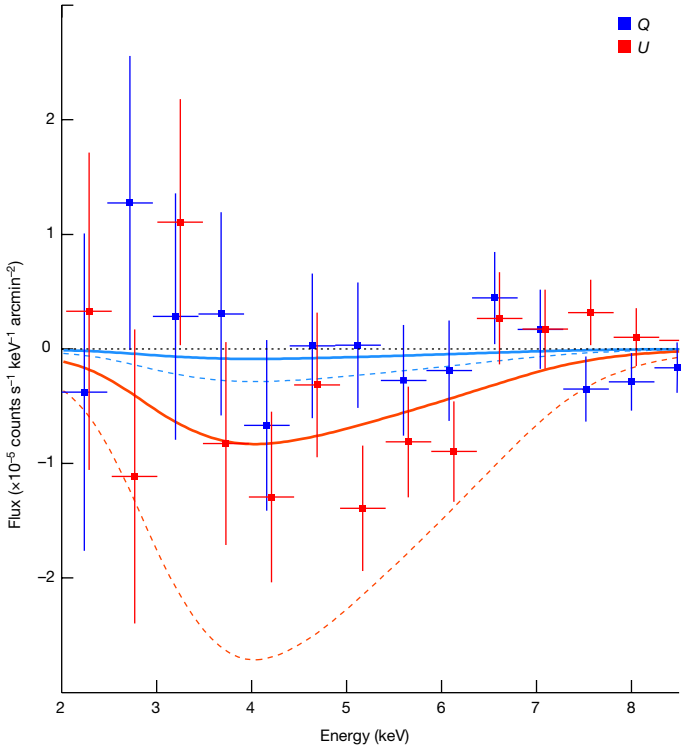

Fig. 3 | Spectra for the Stokes parameters *Q* and *U* extracted from the circular region shown in Fig. 1. The Stokes parameter *Q* is in blue and the *U* parameter is in red. Error bars correspond to 1σ (68% confidence intervals). For clarity, both the *Q* and *U* data points are slightly shifted in energy. The solid blue and red lines represent the best-fitting reflection model (the Compton-scattered continuum component alone) to the *Q* and *U* spectra with a degree of polarization 31% and the polarization angle −48°. The model has been convolved with the IXPE spectral response. The thinner dashed lines are representative of the maximum *Q* and *U* that one could expect for 90° scattering that would lead to a 100%-polarized reflected continuum.

for a short flare, a cloud located behind Sgr A* will remain bright longer than the same cloud in front of it, and therefore, on average, the chances to spot it in a bright phase are higher. Second, the 'younger' flare from Sgr A* would have been observed directly. Indeed, the Advanced Satellite for Cosmology and Astrophysics was active 30 years ago; the giant molecular clouds were bright at the time[5,17], whereas Sgr A* was not. The Sgr B2 cloud, which in the sky plane is much further away from Sgr A* than the area covered by IXPE, was bright too. This fact strongly suggests that the flare is substantially older than 30 yr, or that there were multiple flares. Here the former scenario is adopted and is consistent with the range of values found in the literature (100–500 yr, depending on the methods and Galactic Centre regions probed[18–21]).

Our work presents the missing piece of evidence that X-rays from the giant molecular clouds are due to reflection of an intense, yet short-lived flare produced at or nearby Sgr A*. These results can further constrain the past activity of the Galactic Centre. The observational data provide a flare fluence (product of the luminosity L_X and duration Δt of the flare) of a few 10^{47} erg (refs. 12,22). On the basis of previous studies of the X-ray variability of small molecular clouds in reflected emission, the duration of the flare is $\Delta t < 1.6$ yr (ref. 22). Existing observational data[12,22], including those of IXPE (see Methods), suggest that the broadband (1–100 keV) flare luminosity was in the range from a few 10^{39} to about 10^{44} erg s^{-1} (that is, comparable to the X-ray luminosity of Seyfert galaxies)[23,24]. The lower limit comes from the brightest levels of the surface brightness observed over years (see Methods), whereas the upper limit corresponds to the Eddington luminosity of Sgr A*, which could be exceeded in some scenarios. Given the fluence constraint, the lowest luminosity requires a 1–2-year-long flare, whereas the highest luminosity needs only an hour-long outburst.

Potential origins of flares with the needed fluence[25] include accretion-induced collapse of white dwarfs, sub-luminous γ-ray bursts, tidal disruption events or transient accretion onto supermassive black holes not related to tidal disruption. Classes of transients that can be excluded because their luminosities fall short by a factor of 10–100 include giant flares from soft γ-ray repeaters (magnetars), type II supernova breakouts and major outbursts of ultraluminous X-ray sources. The second line of reasoning could come from the comparison of the expected event rates, bearing in mind that the fluence was calculated for the adopted distance between the clouds and Sgr A*, and therefore, the assumption that the source is further away would boost the required fluence. These considerations favour Sgr A* as the prime candidate, especially considering the consistency of its position with the measured polarization degree, although other scenarios are not completely eliminated.

Detection of the faint and diffuse X-ray emission due to reflection from molecular clouds in the Galactic Centre region remains a

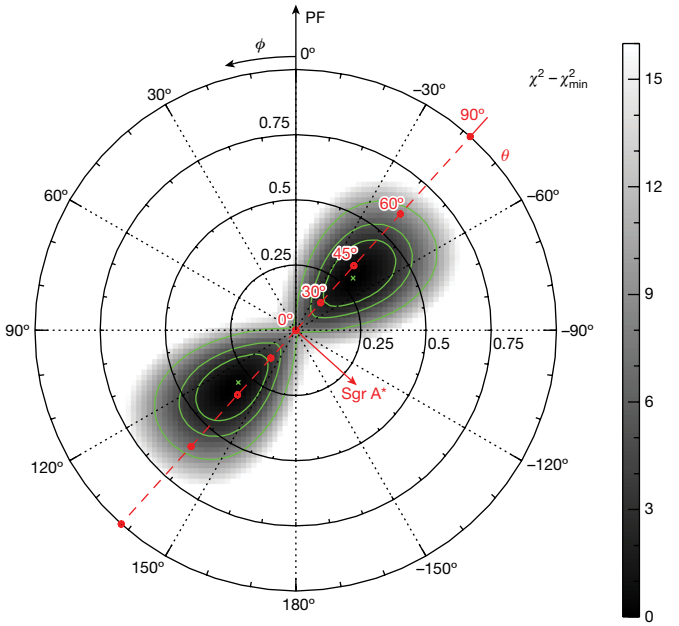

Fig. 4 | Map of the $\chi^2 - \chi^2_{min}$ statistic for the fit of the Stokes parameters *Q* and *U* spectra. We used the reflection continuum model in polar coordinates with radius equal to the polarization fraction (PF) and the azimuthal angle showing the position angle of the electric field vector (ϕ). The minimal value of the statistic χ^2_{min} corresponds to the best-fitting values $\phi = -48°$ and $P = 31\%$ (marked as green crosses), and the contours show 68, 90 and 99% confidence levels. The hypothesis that Sgr A* is the primary source of illuminating X-ray flux implies the polarization angle $\phi = -42°$ for the centre of the region used for extraction of the *Q* and *U* spectra, as marked with the red dashed line. The circles on this line depict expected polarization degrees for the scattering angle changing from 0(180) to 30(150), 45(135), 60(120) and 90 degrees.

challenging exercise. Current IXPE data demonstrate that this goal is within the reach of IXPE, paving a way for future, even longer observations that will enable more detailed analysis, including spatially resolved polarization, to verify the single-flare scenario, and the determination of the intrinsic polarization of the flares to probe the origin of the radiation and constraints on the multiple-flare scenarios.

Online content

Any methods, additional references, Nature Portfolio reporting summaries, source data, extended data, supplementary information, acknowledgements, peer review information; details of author contributions and competing interests; and statements of data and code availability are available at https://doi.org/10.1038/s41586-023-06064-x.

1. Genzel, R., Eisenhauer, F. & Gillessen, S. The Galactic Center massive black hole and nuclear star cluster. *Rev. Mod. Phys.* **82**, 3121–3195 (2010).
2. Vainshtein, L. A. & Syunyaev, R. A. The K-alpha lines in the background X-ray spectrum and the interstellar gas in galaxies. *Sov. Astron. Lett.* **6**, 353–356 (1980).
3. Sunyaev, R. A., Markevitch, M. & Pavlinsky, M. The center of the Galaxy in the recent past: a view from GRANAT. *Astrophys. J.* **407**, 606 (1993).
4. Markevitch, M., Sunyaev, R. A. & Pavlinsky, M. Two sources of diffuse X-ray emission from the Galactic Centre. *Nature* **364**, 40–42 (1993).
5. Koyama, K. et al. ASCA view of our Galactic Center: remains of past activities in X-rays? *Publ. Astron. Soc. Jpn* **48**, 249–255 (1996).
6. Churazov, E., Sunyaev, R. & Sazonov, S. Polarization of X-ray emission from the Sgr B2 cloud. *Mon. Not. R. Astron. Soc.* **330**, 817–820 (2002).
7. Khabibullin, I., Churazov, E. & Sunyaev, R. SRG/eROSITA view of X-ray reflection in the Central Molecular Zone: a snapshot in September-October 2019. *Mon. Not. R. Astron. Soc.* **509**, 6068–6076 (2022).
8. Revnivtsev, M. et al. Discrete sources as the origin of the Galactic X-ray ridge emission. *Nature* **458**, 1142–1144 (2009).
9. Di Gesu, L. et al. Prospects for IXPE and eXTP polarimetric archaeology of the reflection nebulae in the Galactic center. *Astron. Astrophys.* **643**, A52 (2020).
10. Ferrazzoli, R. et al. Prospects for a polarimetric mapping of the Sgr A molecular cloud complex with IXPE. *Astron. Astrophys.* **655**, A108 (2021).
11. Wang, Q. D., Lu, F. & Lang, C. C. X-ray thread G0.13-0.11: a pulsar wind nebula? *Astrophys. J.* **581**, 1148–1153 (2002).
12. Churazov, E., Khabibullin, I., Ponti, G. & Sunyaev, R. Polarization and long-term variability of Sgr A* X-ray echo. *Mon. Not. R. Astron. Soc.* **468**, 165–179 (2017).
13. Marin, F., Muleri, F., Soffitta, P., Karas, V. & Kunneriath, D. Reflection nebulae in the Galactic center: soft X-ray imaging polarimetry. *Astron. Astrophys.* **576**, A19 (2015).
14. Kislat, F., Clark, B., Beilicke, M. & Krawczynski, H. Analyzing the data from X-ray polarimeters with Stokes parameters. *Astropart. Phys.* **68**, 45–51 (2015).
15. Khabibullin, I., Churazov, E. & Sunyaev, R. Impact of intrinsic polarization of Sgr A* historical flares on (polarization) properties of their X-ray echoes. *Mon. Not. R. Astron. Soc.* **498**, 4379–4385 (2020).
16. Sunyaev, R. & Churazov, E. Equivalent width, shape and proper motion of the iron fluorescent line emission from molecular clouds as an indicator of the illuminating source X-ray flux history. *Mon. Not. R. Astron. Soc.* **297**, 1279–1291 (1998).
17. Yamauchi, S., Maeda, Y. & Koyama, K. ASCA observation of the Galactic Center. *Adv. Space Res.* **19**, 63–70 (1997).
18. Ryu, S. G., Koyama, K., Nobukawa, M., Fukuoka, R. & Tsuru, T. G. An X-ray face-on view of the Sagittarius B molecular clouds observed with Suzaku. *Publ. Astron. Soc. Jpn* **61**, 751 (2009).
19. Ryu, S. G. et al. X-ray echo from the Sagittarius C complex and 500-year activity history of Sagittarius A*. *Publ. Astron. Soc. Jpn* **65**, 33 (2013).
20. Terrier, R. et al. Fading hard X-ray emission from the Galactic Center molecular cloud Sgr B2. *Astrophys. J.* **719**, 143–150 (2010).
21. Chuard, D. et al. Glimpses of the past activity of Sgr A* inferred from X-ray echoes in Sgr C. *Astron. Astrophys.* **610**, A34 (2018).
22. Churazov, E., Khabibullin, I., Sunyaev, R. & Ponti, G. Can Sgr A* flares reveal the molecular gas density PDF? *Mon. Not. R. Astron. Soc.* **471**, 3293–3304 (2017).
23. Ptak, A. in *X-ray Astronomy: Stellar Endpoints, AGN, and the Diffuse X-ray Background* Vol. 599 (eds White, N. E. et al.), 326–335 (American Institute of Physics, 2001).
24. Halderson, E. L., Moran, E. C., Filippenko, A. V. & Ho, L. C. The soft X-ray properties of nearby low-luminosity active galactic nuclei and their contribution to the cosmic X-ray background. *Astron. J.* **122**, 637–652 (2001).
25. Soderberg, A. et al. in *astro2010: The Astronomy and Astrophysics Decadal Survey* Vol. 2010 (NASA, 2009).
26. Weisskopf, M. C. et al. The Imaging X-Ray Polarimetry Explorer (IXPE): pre-launch. *J. Astron. Telesc. Instrum. Syst.* **8**, 026002 (2022).

[1]Université de Strasbourg, CNRS, Observatoire Astronomique de Strasbourg, UMR 7550, Strasbourg, France. [2]Max Planck Institute for Astrophysics, Garching, Germany. [3]Space Research Institute of the Russian Academy of Sciences, Moscow, Russia. [4]Universitäts-Sternwarte, Fakultät für Physik, Ludwig-Maximilians-Universität München, Munich, Germany. [5]INAF Istituto di Astrofisica e Planetologia Spaziali, Rome, Italy. [6]ASI - Agenzia Spaziale Italiana, Rome, Italy. [7]Space Science Data Center, Agenzia Spaziale Italiana, Rome, Italy. [8]INAF Osservatorio Astronomico di Roma, Monte Porzio Catone, Italy. [9]Center for Astrophysics, Harvard & Smithsonian, Cambridge, MA, USA. [10]Dipartimento di Matematica e Fisica, Università degli Studi Roma Tre, Rome, Italy. [11]Université Grenoble Alpes, CNRS, IPAG, Grenoble, France. [12]RIKEN Cluster for Pioneering Research, Wako, Japan. [13]Instituto de Astrofísica de Andalucía-CSIC, Granada, Spain. [14]INAF Osservatorio Astronomico di Cagliari, Selargius, Italy. [15]Istituto Nazionale di Fisica Nucleare, Sezione di Pisa, Pisa, Italy. [16]Dipartimento di Fisica, Università di Pisa, Pisa, Italy. [17]NASA Marshall Space Flight Center, Huntsville, AL, USA. [18]Istituto Nazionale di Fisica Nucleare, Sezione di Torino, Turin, Italy. [19]Dipartimento di Fisica, Università degli Studi di Torino, Turin, Italy. [20]INAF Osservatorio Astrofisico di Arcetri, Florence, Italy. [21]Dipartimento di Fisica e Astronomia, Università degli Studi di Firenze, Sesto Fiorentino, Italy. [22]Istituto Nazionale di Fisica Nucleare, Sezione di Firenze, Sesto Fiorentino, Italy. [23]Science and Technology Institute, Universities Space Research Association, Huntsville, AL, USA. [24]Istituto Nazionale di Fisica Nucleare, Sezione di Roma "Tor Vergata", Rome, Italy. [25]Department of Physics and Kavli Institute for Particle Astrophysics and Cosmology, Stanford University, Stanford, CA, USA. [26]Institut für Astronomie und Astrophysik, Universität Tübingen, Tübingen, Germany. [27]Astronomical Institute of the Czech Academy of Sciences, Prague 4, Czech Republic. [28]California Institute of Technology, Pasadena, CA, USA. [29]Yamagata University, Yamagata-shi, Japan. [30]Osaka University, Suita, Japan. [31]University of British Columbia, Vancouver, British Columbia, Canada. [32]School of Mathematics, Statistics and Physics, Newcastle University, Newcastle upon Tyne, UK. [33]Department of Physics, Faculty of Science and Engineering, Chuo University, Tokyo, Japan. [34]International Center for Hadron Astrophysics, Chiba University, Chiba, Japan. [35]Institute for Astrophysical Research, Boston University, Boston, MA, USA. [36]Department of Astrophysics, St. Petersburg State University, St Petersburg, Russia. [37]Department of Physics and

Astronomy, University of Iowa, Iowa City, IA, USA. [38]Physics Department and McDonnell Center for the Space Sciences, Washington University in St. Louis, St Louis, MO, USA. [39]Finnish Centre for Astronomy with ESO, University of Turku, Turku, Finland. [40]MIT Kavli Institute for Astrophysics and Space Research, Massachusetts Institute of Technology, Cambridge, MA, USA. [41]Graduate School of Science, Division of Particle and Astrophysical Science, Nagoya University, Nagoya, Japan. [42]Hiroshima Astrophysical Science Center, Hiroshima University, Higashi-Hiroshima, Japan. [43]University of Maryland, Baltimore County, Baltimore, MD, USA. [44]NASA Goddard Space Flight Center, Greenbelt, MD, USA. [45]Center for Research and Exploration in Space Science and Technology, NASA/GSFC, Greenbelt, MD, USA. [46]Department of Physics, The University of Hong Kong, Pokfulam, Hong Kong. [47]Department of Astronomy and Astrophysics, Pennsylvania State University, University Park, PA, USA. [48]Department of Physics and Astronomy, University of Turku, Turku, Finland. [49]INAF Osservatorio Astronomico di Brera, Merate, Italy. [50]Dipartimento di Fisica e Astronomia, Università degli Studi di Padova, Padua, Italy. [51]Dipartimento di Fisica, Università degli Studi di Roma "Tor Vergata", Rome, Italy. [52]Department of Astronomy, University of Maryland, College Park, MD, USA. [53]Mullard Space Science Laboratory, University College London, Dorking, UK. [54]Anton Pannekoek Institute for Astronomy & GRAPPA, University of Amsterdam, Amsterdam, The Netherlands. [55]Guangxi Key Laboratory for Relativistic Astrophysics, School of Physical Science and Technology, Guangxi University, Nanning, China. ✉e-mail: frederic.marin@astro.unistra.fr

Methods

IXPE and Chandra observation

The molecular complex Sgr A is the brightest collection of reflection clouds in X-ray emission around Sgr A* at present[7]. This region, centred on right ascension 266.51° and declination −28.89° in equatorial coordinates, was pointed by IXPE[26] with a total integration time of 0.93 Ms (324 ks from 27 February to 6 March 2022, and 639 ks from 10 to 24 March 2022), after filtering for episodes of enhanced instrumental background.

In addition to the X-ray polarimetric data, a few quasi-simultaneous observations with the Chandra X-ray observatory were acquired from 26 February to 11 March 2022 using the Advanced CCD Imaging Spectrometer (ACIS)-I detector (observation IDs 24373, 24820 and 26353), which cover the 0.3–10.0-keV band with a spectral resolution of $\Delta E \approx 0.3$ keV near $E = 6$ keV and arcsecond angular resolution. The Chandra high-angular-resolution data were essential to identify regions where the reflected emission is strong and to extract spectra from these regions.

IXPE data reduction

The IXPE observatory, as described in detail in ref. 26, includes three identical X-ray telescopes, each comprising an X-ray mirror module assembly (provided by the National Aeronautics and Space Administration (NASA)) and a polarization-sensitive gas pixel detector (provided by the Italian side of the collaboration), to offer spatially resolved X-ray polarimetry in the 2–8-keV energy band. At the Science Operations Center (at the NASA Marshall Space Flight Center), a software pipeline developed jointly by the Italian Space Agency (Agenzia Spaziale Italiana (ASI)) and NASA processes the relevant science, engineering and ancillary data, and estimates the photoelectron emission direction (and hence the polarization), position and energy of each event after applying corrections for charging effects of the gas electron multiplier, detector temperature, and gain non-uniformity. The use of the IXPE on-board calibration sources[27] allows correction for time-dependent and spatially dependent gain variations of the detectors. The in-flight calibration measurements provide the best knowledge of the gain of the detectors at the time of the observation, and hence the correct energy of each photon, needed to correct the Stokes parameters for the presence of spurious polarization, and to use the correct value of the modulation factor (the modulation amplitude for radiation that is 100% linearly polarized[26]). The removal of spurious polarization is achieved using the algorithm of ref. 28.

The output of this pipeline processing is an event file in FITS format for each of the three IXPE detector units that, in addition to the typical information related to spatially resolved X-ray astronomy, contains the event-by-event Stokes parameters (see ref. 14) from which the polarization of the radiation can be derived. The data products are archived at the High-Energy Astrophysics Science Archive Research Center (HEASARC, at the NASA Goddard Space Flight Center), for use by the international astrophysics community. These level-2 event files were cleaned from additional environmental and background contamination (A.D.M. et al., manuscript in preparation).

In the case of the observation of the Galactic Centre, the observation window corresponded to a period of increased solar activity that led to an increase of atmospheric noise (particle background). In addition, such activity tends to extend the South Atlantic Anomaly (SAA), above which the detectors are usually turned off to prevent observation in a highly particle-polluted environment. However, as can be seen in Extended Data Fig. 1 a, several spikes were recorded in the light curve right before the spacecraft entry in the SAA. Using the v26.0.0 ixpeobssim tool (available at https://ixpeobssim.readthedocs.io/en/latest/)[29], we removed the count spikes associated with Earth occultation periods and above the extended SAA. Some spurious events attributed to geomagnetic storm events were also flagged and excised. New good time intervals were then computed using these prolonged epochs and allowed event filtering based on the presence of unaccounted atmospheric noise. After good time interval correction (Extended Data Fig. 1c), the livetime (or total good time) is 0.93 Ms, which represents 96.7% of the livetime before filtering.

IXPE systematic effects

All systematic errors are well below the polarization degree and angle observed from the 4.5′ extraction circle we used in this paper. Below, we give a brief statement on each of the sources of potential systematic effects and refer to the pre-launch papers for a deeper analysis[30] (A.D.M. et al., manuscript in preparation).

Instrumental and extragalactic backgrounds. From the stacking of almost 2 million seconds' worth of background-rejected data from annular background regions around extragalactic point sources (see Extended Data Table 1; we also excluded sources bright enough to pollute the background extraction region with their signal because of the wing of the point spread function), the background is unpolarized down to a minimum detectable polarization of 3.7% at 99% confidence level. This is well below the measured polarization from the Sgr A region presented in this work.

Spurious polarization. The spurious polarization we managed to calibrate in a 4.5′ radius amounts to 0.05%. The statistical error on the derived polarization measurement is 11% (or about 4% modulation). As a consequence, the residual systematic polarization has no effect on the results presented in this paper.

Stray light. The IXPE requirement on the level of stray light is that its suppression should be larger than a factor of 200 (verified at 2.3 keV). We rescaled the suppression coefficient of the three more intense sources outside the 4.5′-radius circle used in this paper as found in the Chandra catalogue (see Extended Data Table 2). The resulting stray-light counting rate (0.5–7 keV) from these sources outside the field of view is 10 μCrab at most (Crab 0.5–7 keV = 2.8×10^{-8} erg s^{-1} cm^{-2}). Assuming that these sources are 10% polarized, the effect on the observed counting rate is at most 0.1% (that is, negligible).

Solar effects. Owing to the thick shielding of the detectors, only in the case of a very bright X Class solar flare, a few photons have been detected (cross-matched by monitoring satellites). Data in coincidence of solar flares are simply removed. In addition, spikes due to passages over the SAA were also removed, as stated previously, and thus do not contribute to systematic effects.

Effects related to Earth's atmosphere. The Earth's atmosphere, during most of the observations, crosses the field of view of the IXPE at each orbit. The data are excluded from the analysis. In any case, the atmosphere is dark in the range of the IXPE and becomes bright above 10 keV. Thus, we can state that the albedo of Earth is never directly observed by IXPE telescopes. Indirectly, namely through scattering, it contributes to the instrumental background. In fact, the satellite orbits the Earth with an angular velocity of 360° in 90 min, which is 4° per minute. This means that the source is seen on the limb of the Earth only within 13′, which is 3 s each orbit.

Chandra data reduction

The Chandra data reduction follows a standard procedure based on the latest versions of the data reduction software (CIAO v4.14) and calibration (CALDB v4.9.8). Our particular approach and analysis steps are described in detail in ref. 31. Briefly, they include identification and removal of high-background periods, correction of photon energies for the time and detector temperature dependence of the charge transfer

inefficiency and gain, and creation of matching background datasets using blank-sky observations with exposure times similar to those of the Galactic Centre pointings.

The Chandra observing programme included multiple pointings with individual exposures of 10–30 ks. Owing to the spacecraft orientation relative to the Sun, many observations were carried out with the ACIS focal plane temperature substantially higher than a nominal value of −120 °C, resulting in potential problems with the detector gain and response calibration. To minimize the impact of this issue, we have used three Chandra pointings (observation IDs 24373, 24820 and 26353) with the lowest focal plane temperatures ($T < -116.5$ °C) and that were carried out quasi-simultaneously with the IXPE observations (26 February to 11 March), with a total exposure of 52 ks.

For the analysis presented here, we use the combined flat-fielded and background-subtracted Chandra image in the 4–8-keV band, and spectra extracted in 4.5′ circular region discussed above. Following the standard approach for analysing Chandra spectra of extended sources, we have generated the spectral response files that combine the position-dependent ACIS calibration with the weights proportional to the observed brightness in the 4–8-keV band. The extracted spectral data and response files are fitted to a set of models as described below.

To assess the impact of the calibration uncertainties associated with the elevated focal plane temperature, we repeated all analyses using the observation IDs with higher temperatures than the three pointings used in this work. These experiments have shown that after the standard temperature-dependent corrections implemented in CIAO, the parameters of interest for this work (for example, the 4–8-keV flux of the reflected component) are almost unchanged. Therefore, we conclude that the impact of elevated focal plane temperatures on our analysis is negligible.

Archival observations with XMM-Newton

To better constrain spectral decomposition of the X-ray emission from the region of interest, we have used all archival observations with the XMM-Newton observatory accumulated between 2002 and 2012. These data have already been used for studies of the reflection component[12]. The XMM-Newton data were prepared, reduced and processed in exactly the same manner. As the final step, the spectrum was extracted from the same region as used by IXPE. Owing to the large effective area above 4 keV and long total exposure time supplemented with superior spectral resolution around 6 keV, the XMM-Newton data allow us to better separate thermal and reflected components. As only the contribution of the reflected component is expected to vary over time, one can combine the archival data with the quasi-simultaneous Chandra and IXPE observations by allowing only parameters of the reflected component model to vary while linking parameters of all other components when fitting the spectra of the total emission observed by all three observatories.

Combined analysis of IXPE, Chandra and XMM-Newton data

As the first step of the joint IXPE, Chandra and XMM-Newton analysis, the background-subtracted spectra extracted from the circular region shown in Fig. 1 have been fitted with the same multi-component model.

This model includes a reflection component and three ‘thermal’ components (an illustrative example of the spectral model is shown in Extended Data Fig. 2). The latter components can be approximated as emission of optically thin thermal plasma, even though they might now be indeed associated with diffuse X-ray emitting gas. Indeed, in the 4–8-keV energy band, the most important is the thermal component with temperature $kT \approx 6$ keV, which is plausibly due to cumulative emission of a large number of point sources, mostly accreting white dwarfs and stars with active coronae[8]. The APEC model (see http://www.atomdb.org/) was used for the optically thin thermal components. The reflection component describes the spectrum emerging from a spherical cloud of molecular gas, illuminated by a beam of X-rays, having a power-law spectrum. For this purpose, a publicly available CREFL16 model[12] was used, and more specifically a version of it in which reflected continuum and fluorescent lines are treated separately but with tied parameters. CREFL16 is a model describing the spectrum of a uniform gas cloud illuminated by a parallel beam of X-rays. The model covers the energy range from 0.3 to 100 keV. It has five parameters: the Thomson optical depth of the cloud, the photon index of the incident spectrum, the abundance of heavy elements, the cosine of the angle between the line of sight and the illuminating angle, and the normalization. The softer thermal components are needed to properly describe the line-rich spectrum at energies below 3–4 keV (Fig. 2). Similarly to the hotter component discussed above, the exact nature of these components is still a matter of debate[32].

A combination of all components provides a reasonably good approximation of the IXPE, Chandra and archival XMM-Newton spectra extracted from the reference region. XSPEC version 12.10.1f was used for fitting the spectra of Chandra, XMM-Newton and IXPE. For IXPE, XSPEC was also used to fit the Q and U spectra, too. We note in passing that IXPE and Chandra observations are quasi-simultaneous, whereas the XMM-Newton data were averaged over several observations spread over many years (from 2002 to 2012). For that reason, the normalization of the reflected component in the XMM-Newton model was decoupled from the IXPE and Chandra models. All other components and parameters were tied across all three instruments. A standard χ^2 minimization has been used to fit all spectra (polarized and total). This approach is suitable for the IXPE, XMM-Newton and Chandra datasets used here. The best-fitting spectral model (Fig. 2) to the combined dataset of three instruments has a $\chi^2 = 1{,}400$ for 922 degrees of freedom. The residuals shown in the second panel of Fig. 2 are of the order of about 20%, providing a reasonable approximation of the data. The excess of the χ^2 above expectations ($\chi^2 = 922 \pm 43$ at the 68% confidence) for the genuine model is not surprising given the simplicity of the model used here and, also, modest cross-calibration issues among all three telescopes.

The outcome of the spectral fitting model was in particular the normalization of the reflected component (expressed in units of surface brightness) and the parameters of the best-fitting CREFL16 model, which do not substantially affect the results of the IXPE data analysis. Critically assessing the spectral decomposition shown in Fig. 2, we concluded that a systematic uncertainty of order 30% is associated with the derived normalization of the reflected component. As only the scattered continuum of the reflected component is polarized (ignoring second-order effects caused by multiple scatterings,[6,33]), it was singled out and used to fit Q and U spectra measured by IXPE as shown in Fig. 3. For that fit, the scattered continuum component was multiplied by the effective area appropriate for the extraction region (taking into account vignetting) and the modulation factor. For Q and U spectra, the dependence on the polarization angle ϕ was accounted for by introducing multiplicative factors $\cos 2\phi$ and $\sin 2\phi$ in front of the scattered continuum component, for Q and U, respectively. Namely, for the Thomson scattering,

$$Q(E) = P\cos 2\phi \times S(E)$$
$$U(E) = P\sin 2\phi \times S(E),$$

in which $S(E)$ is the spectrum of the scattered continuum as derived from the spectral analysis, and P is the degree of polarization. This model is valid in the single-scattering approximation, and for a compact scattering cloud. From these expressions, it is clear that P is degenerate with the normalization of $S(E)$, but it does not affect the detection significance of non-zero polarization. This allows one to use a multiplicative notation when quoting the polarization degree

as $P = (31 \pm 11)\% \times (1 \pm 0.3)$, in which the second term arises from the uncertainties in the reflected continuum normalization.

The best-fitting model to the Q and U spectra (Fig. 3) has a $\chi^2 = 254.4$ for 248 unbinned channels and two free parameters—the normalization of the polarized component and the polarization angle. In the figure, the channels were grouped (12 channels per bin) for display purposes.

Sgr A* flare parameters

More than a century ago, it was realized[34] that for a flare of a compact source and an arbitrary observer, its scattered light with a given time delay since the moment of the flare is associated with the matter located on the surface of an ellipsoid of rotation. The source and the observer are at the foci of the ellipsoid. Furthermore, in close vicinity of the source, the ellipsoid can be approximated by a paraboloid. Assuming that Sgr A* is the primary source, a detection of the scattered light from a cloud relates the age of the flare and the position of the cloud as

$$t = \frac{\sqrt{x^2 + z^2}}{c} + \frac{z}{c}, \quad (1)$$

in which c is the speed of light, and x and z are the distances of the cloud from Sgr A* in the sky plane and along the line of sight, respectively.

The degree of polarization P depends on the cosine of the scattering angle μ (in the limit of Thomson scattering) as

$$P = \frac{1 - \mu^2}{1 + \mu^2}, \quad (2)$$

in which

$$\mu = -\frac{z}{\sqrt{x^2 + z^2}}. \quad (3)$$

Thus, knowing P, one can reconstruct the three-dimensional position of illuminated clouds. For instance, for $x = 25$ pc and $\theta = 137°$, $z \approx 26$ pc (that is, the illuminated clouds are further away from us than Sgr A* by this distance). Combining the above three equations, one can explicitly relate the delay time t and the measured degree of polarization P

$$t = \frac{x}{c} \times \left[\left(\frac{1+P}{2P} \right)^{1/2} \pm \left(\frac{1-P}{2P} \right)^{1/2} \right]. \quad (4)$$

This expression was used to estimate the age of the flare.

The determination of the flare luminosity is notoriously difficult, as it depends not only on the distance of the cloud from Sgr A*, but also on the density of the cloud gas and the duration of the flare. One can partly circumvent this problem by using the maximal possible albedo of a molecular cloud[12] to convert the observed X-ray surface brightness into a lower limit on the luminosity

$$L_{4-8,\min} = \frac{I_{4-8}}{\eta_{\max}} 4\pi D_{\rm sc}^2 \approx 8 \times 10^{37} \text{ erg s}^{-1}, \quad (5)$$

in which $I_{4-8} = 4.6 \times 10^{-13}$ erg s^{-1} cm^{-2} arcmin^{-2} $= 5.4 \times 10^{-6}$ erg s^{-1} cm^{-2} sr^{-1} is the observed flux from the studied region[7], $\eta_{\max} \approx 10^{-2}$ is the maximal albedo, and $D_{\rm sc} = \sqrt{x^2 + z^2} \approx 36$ pc is the distance between Sgr A* and the clouds. Conversion of $L_{4-8,\min}$ to a broader 1–100-keV band assuming a power-law spectrum with the photon index of 2.0 (the value typically measured for the Sgr A giant molecular clouds[35]) yields $L_{1-100,\min} \approx 6 \times 10^{38}$ erg s^{-1}. If the optical depth or, equivalently, the hydrogen column density of illuminated clouds is known, one can use the real albedo in the above equation, driving the minimum luminosity up. Similarly, if only a fraction of the area of the studied region is covered by illuminated clouds, the true luminosity will be higher. For instance, focusing on individual bright clouds drives this estimate up by an order of magnitude to the level of a few 10^{39} erg s^{-1} (ref. 12), and this is still a lower limit.

However, there is no easy way of placing an upper limit on the source luminosity (for a short flare) without additional explicit assumptions on the gas density and the duration of the flare. For instance, an hour-long flare with a luminosity of about 10^{44} erg s^{-1} could be consistent with the data.

Finally, we note that the above derivation assumes that all visible reflection emission is due to a single flare. If Sgr A* produced multiple flares over the past several hundred years[21,36], then the fluxes and polarization will be affected. Longer IXPE observations should be able to test this scenario by providing a polarization measurement of individual giant molecular clouds.

Data availability

The IXPE data that support the findings of this study are freely available in the HEASARC IXPE data archive (https://heasarc.gsfc.nasa.gov/docs/ixpe/archive/). The XMM-Newton data can be found on the same website, and the Chandra data will be public after one year from the observation date.

Code availability

The analysis and simulation software ixpeobssim developed by the IXPE collaboration and its documentation are available publicly through https://ixpeobssim.readthedocs.io/en/latest/?badge=latest.494. XSPEC is distributed and maintained under the aegis of the HEASARC and can be downloaded as part of HEAsoft from http://heasarc.gsfc.nasa.gov/docs/software/lheasoft/download.html.

27. Ferrazzoli, R. et al. In-flight calibration system of Imaging X-ray Polarimetry Explorer. *J. Astron. Telesc. Instrum. Syst.* **6**, 048002 (2020).
28. Rankin, J. et al. An algorithm to calibrate and correct the response to unpolarized radiation of the X-ray polarimeter onboard IXPE. *Astron. J.* **163**, 39 (2022).
29. Baldini, L. et al. ixpeobssim: a simulation and analysis framework for the imaging X-ray polarimetry explorer. *SoftwareX* **19**, 101194 (2022).
30. Muleri, F. et al. in *Space Telescopes and Instrumentation 2016: Ultraviolet to Gamma Ray* Vol. 9905 (eds den Herder, J.-W. A. et al.) 99054G (Society of Photo-Optical Instrumentation Engineers, 2016).
31. Vikhlinin, A. et al. Chandra Cluster Cosmology Project. II Samples and X-ray data reduction. *Astrophys. J.* **692**, 1033–1059 (2009).
32. Yuasa, T., Makishima, K. & Nakazawa, K. Broadband spectral analysis of the Galactic Ridge X-ray emission. *Astrophys. J.* **753**, 129 (2012).
33. Marin, F., Karas, V., Kunneriath, D. & Muleri, F. Prospects of 3D mapping of the Galactic Centre clouds with X-ray polarimetry. *Mon. Not. R. Astron. Soc.* **441**, 3170–3176 (2014).
34. Kapteyn, J. C. On the motion of Nebulae in vicinity of Nova Persei. *Pop. Astron.* **10**, 124–127 (1902).
35. Ponti, G., Terrier, R., Goldwurm, A., Belanger, G. & Trap, G. Discovery of a superluminal Fe K echo at the Galactic Center: the glorious past of Sgr A* preserved by molecular clouds. *Astrophys. J.* **714**, 732–747 (2010).
36. Clavel, M. et al. Echoes of multiple outbursts of Sagittarius A* revealed by Chandra. *Astron. Astrophys.* **558**, A32 (2013).
37. Sidoli, L. & Mereghetti, S. The X-ray diffuse emission from the Galactic Center. *Astron. Astrophys.* **349**, L49–L52 (1999).

Acknowledgements The IXPE is a joint US and Italian mission. The US contribution is supported by NASA and led and managed by its Marshall Space Flight Center, with industry partner Ball Aerospace (contract NNM15AA18C). The Italian contribution is supported by ASI through contract ASI-OHBI-2017-12-I.0, agreements ASI-INAF-2017-12-H0 and ASI-INFN-2017.13-H0, and its Space Science Data Center with agreements ASI-INAF-2022-14-HH.0 and ASI-INFN 2021-43-HH.0, and by the Istituto Nazionale di Astrofisica and the Istituto Nazionale di Fisica Nucleare in Italy. This research used data products provided by the IXPE team (the Marshall Space Flight Center, the Space Science Data Center, the Istituto Nazionale di Astrofisica and the Istituto Nazionale di Fisica Nucleare) and distributed with additional software tools by the HEASARC, at the NASA Goddard Space Flight Center. F.M. is grateful to the Astronomical Observatory of Strasbourg, the Centre National de la Recherche Scientifique and the University of Strasbourg under whose benevolence this paper was written. I.K. acknowledges support by the COMPLEX project from the European Research Council under the European Union's Horizon 2020 research and innovation programme grant agreement ERC-2019-AdG 882679. P.-O.P. acknowledges financial support from the French National Program of High Energy (PNHE)/Centre National de la Recherche Scientifique and from the French national space agency (Centre National d'Etudes Spatiales (CNES)). I.A. acknowledges financial support from the Spanish Ministerio de Ciencia e Innovación (MCIN/AEI/

10.13039/501100011033) through the Center of Excellence Severo Ochoa award for the Instituto de Astrofísica de Andalucía-CSIC (CEX2021-001131-S), and through grants PID2019-107847RB-C44 and PID2022-139117NB-C44. A.I. acknowledges support from the Royal Society. A.V., W.F. and R.K. acknowledge support from NASA grant GO1-22136X, the Smithsonian Institution, and the Chandra High Resolution Camera Project through NASA contract NAS8-03060. C.-Y.N. is supported by a GRF grant of the Hong Kong Government under HKU 17305419.

Author contributions F.M. led the IXPE observation, contributed to the analysis and led the writing of the paper. E. C., I.K., R.F., L.D.G., T.B., A.D.M., R.M., E.C., P.S., F.M., R.S. and P.K. contributed to the IXPE analysis, discussion and writing of the paper. A.V., W.F. and R.K. provided and reduced the Chandra data used in this paper. S.B., I.D., P.-O.P. and T.E. contributed with discussion and parts of the paper. The remaining authors are part of the IXPE team whose substantial contribution made the satellite and the Galactic Centre observation possible.

Competing interests The authors declare no competing interests.

Additional information

Supplementary information The online version contains supplementary material available at https://doi.org/10.1038/s41586-023-06064-x.

Correspondence and requests for materials should be addressed to Frédéric Marin.

Peer review information *Nature* thanks Rozenn Boissay-Malaquin and Gabriele Ponti for their contribution to the peer review of this work. Peer reviewer reports are available.

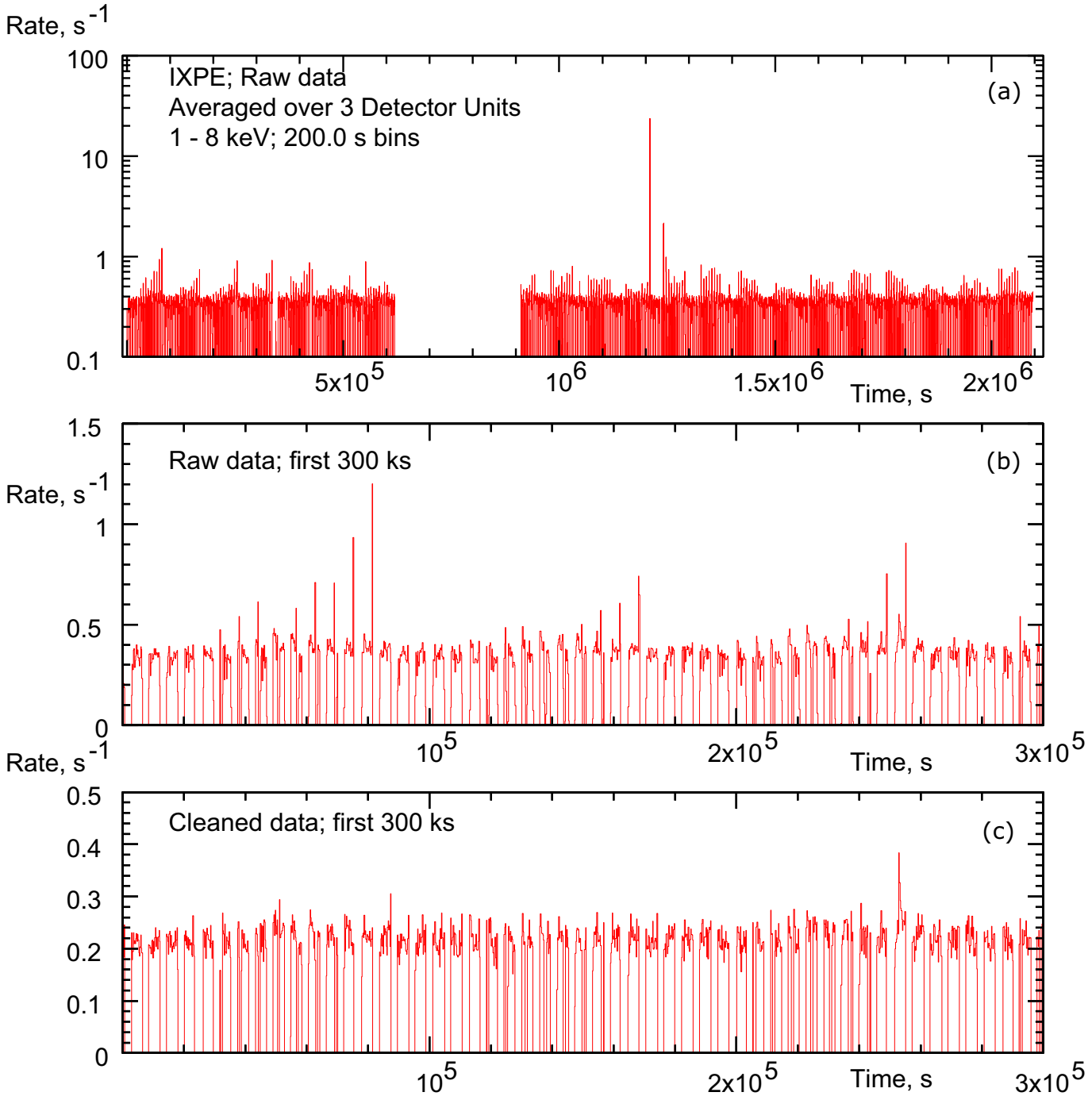

Extended Data Fig. 1 | Illustration of the data cleaning prior to the imaging and spectral analysis. Panel (a) shows the count rate in the 2–8 keV band (sum of three DUs, 200 seconds time bins) in the original data set that spans 2 million seconds. The two most intense spikes are associated with a geomagnetic storm. To illustrate less prominent variations, panel (b) shows a 300 kiloseconds-long portion of the same light curve that feature a number of smaller amplitude quasi-regular spikes (notice that the vertical scale has changed) that are mostly due to the South Atlantic Anomaly. The gaps in the light curves correspond to moments when the Galactic center was obscured by the Earth. Finally, panel (c) shows the count rate for the data cleaned from spikes and individual events that most plausibly are due to detector background rather than X-ray photons. The overall count rate in the cleaned data is almost a factor of two lower than in the original data.

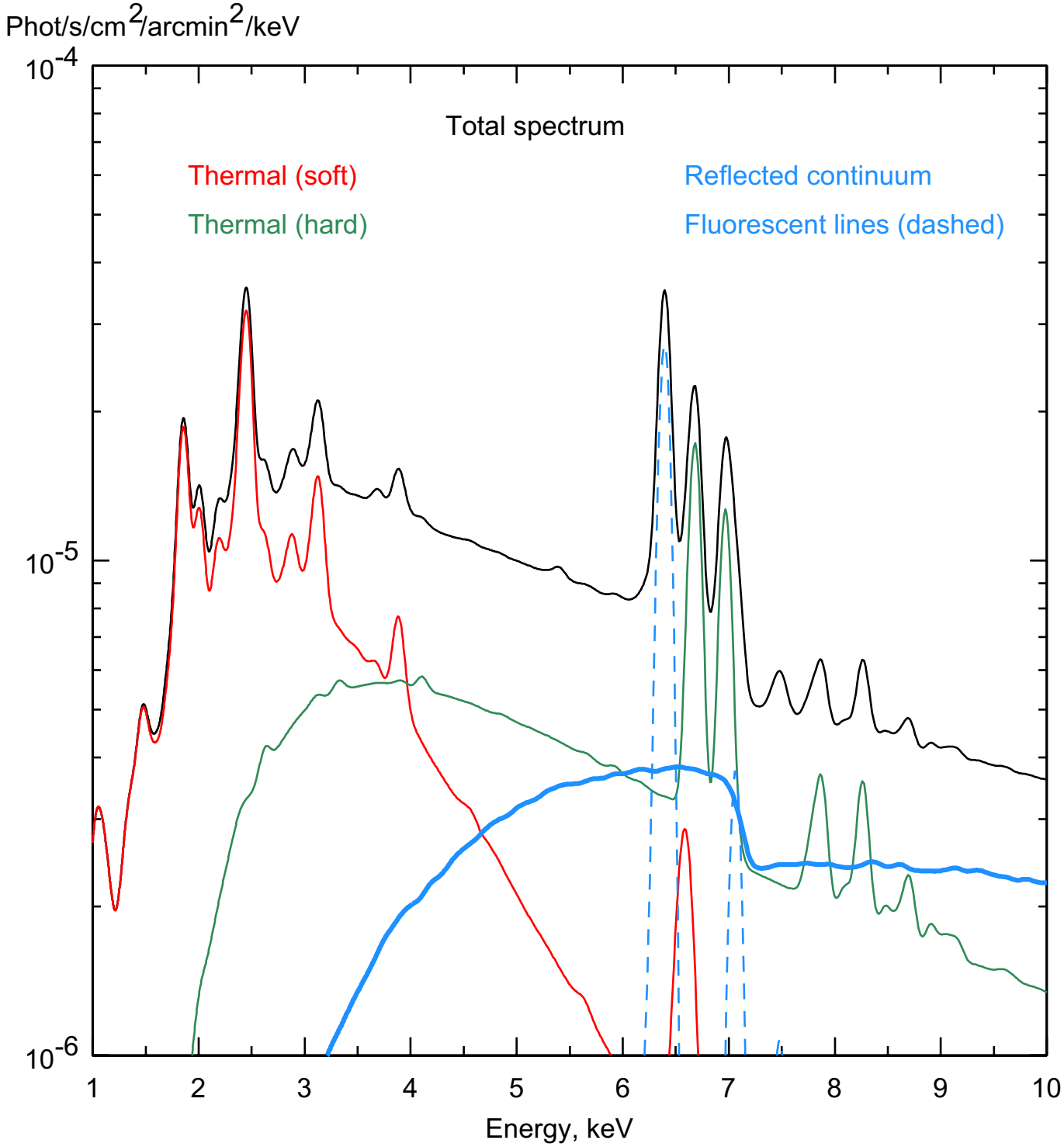

Extended Data Fig. 2 | An illustration of the spectral model used to approximate X-ray spectra extracted from the reference region. For clarity, only two "thermal" components are shown in the plot. The red and the green curves are those thermal components, detailed in[9,37]. The hotter (green) of the models, having prominent lines at 6.7 and 6.97 keV, contributes substantially to the 4–8 keV band. The blue curves show the two components of the reflected emission. Namely, the dashed blue curves show the fluorescent lines of iron (Kα line at 6.4 keV and Kβ line at 7.06 keV), while the thick blue line shows the scattered continuum. Only the latter component is polarized and used to fit the Q and U spectra measured by IXPE. The black line shows the sum of all components. In order to show more clearly the components of the physical model in units of photons s^{-1} cm^{-2} $arcmin^{-2}$ keV^{-1} the spectra were convolved with a Gaussian, which is narrower than the energy resolution of the IXPE, Chandra, and XMM-Newton detectors.

Extended Data Table 1 | Observations used in this work for background extraction

Mission	Obs.ID	Start date (YYYY-MM-DD)	Effective exposure (kiloseconds)	Notes
IXPE	1003701	2022-05-04	96.7	Mrk421
IXPE	1003801	2022-06-04	96.0	Mrk421
IXPE	1004501	2022-03-08	100.4	Mrk501
IXPE	1004701	2022-07-09	97.8	Mrk501
IXPE	1006301	2022-05-06	390.9	BL Lac
IXPE	1006301	2022-05-06	116.9	BL Lac
IXPE	1003501	2022-07-12	771.8	Circinus
IXPE	1005701	2022-06-12	264.2	3C279

Extended Data Table 2 | The three more intense sources and their rescaled flux in the extraction region we used in our paper (see Fig. 1)

Source	Flux	Angular sep. (°)	Suppression factor	Re-scaled flux
2CXO J174621.1-284343	5.033E-11	0.22	245	1.4E-13
2CXO J174451.6-292042	3.949E-11	0.52	752	3.4E-14
2CXO J174445.4-295045	3.387E-11	0.964	1120	2.0E-14

Fluxes are in erg s^{-1} cm^{-2}.